A TEM and neutron diffraction study of the local structure in the rhombohedral phase of lead zirconate titanate



1998 J. Phys.: Condens. Matter 10 1767

(http://iopscience.iop.org/0953-8984/10/8/011)

J. Phys.: Condens. Matter **10** (1998) 1767–1786. Printed in the UK PII: S0953-8984(98)86992-0

# A TEM and neutron diffraction study of the local structure in the rhombohedral phase of lead zirconate titanate

J Ricote†, D L Corker‡‖, R W Whatmore†, S A Impey†, A M Glazer‡, J Dec§ and K Roleder§

† School of Industrial and Manufacturing Science, Cranfield University, Cranfield, Bedfordshire MK43 0AL, UK

‡ Department of Physics, Clarendon Laboratory, Parks Road, University of Oxford, Oxford OX1 3PU, UK

§ Institute of Physics, Silesian University, Uniwersytecka 4, 40-007 Katowice, Poland

Received 20 August 1997

**Abstract.** Transmission electron microscopy and neutron diffraction have been used to characterize ceramics and single crystals from the rhombohedral region of the $Pb(Zr_{1-x}Ti_x)O_3$ ($x = 0.06$–$0.45$) phase diagram. Electron diffraction patterns showed the existence of superlattice reflections of the type $\frac{1}{2}\{hkl\}_p$, where $h = k = l$, and $\frac{1}{2}\{hk0\}_p$, which are not observed by neutron powder diffraction. The analysis of these reflections also revealed satellite spots around the $\frac{1}{2}\{hk0\}_p$, which are associated with periodic antiphase boundaries. The origin of these superlattice reflections is explained by the existence of local regions presenting antiparallel cation displacements, and models for this are suggested and compared with experiment.

## 1. Introduction

Perovskite ferroelectrics, particularly those of the $PbZrO_3$–$PbTiO_3$ (PZT) system, have been studied extensively for their interesting technological properties and for the light they can shed upon the structural origins of ferroelectricity. The basic oxide perovskite structure possesses the formula $ABO_3$ (the mineral 'perovskite' being $CaTiO_3$) in which the B cations are octahedrally co-ordinated by the oxygens. The structure consists of an infinite framework of corner-linked $BO_6$ octahedra, with the A cations in the spaces between the octahedra. In most perovskites, numerous structural distortions can occur. These can be through cation displacements and/or octahedral rotations and/or distortions. In many cases these exhibit unit-cell doubling and the consequent occurrence of superlattice reflections. For the purposes of this paper, Miller indices will generally be assigned to reflections on the basis of the pseudo-cubic $\approx$4 Å unit cell. These indices will be labelled with the subscript $p$.

In general, there are three possible mechanisms for the generation of superlattice reflections in perovskite diffraction patterns [1]: chemical ordering between cation species, octahedral tilts and antiparallel displacement of cations. The structures of the rhombohedral phases of $Pb(Zr_{1-x}Ti_x)O_3$ solid solutions $0.05 \leqslant x \leqslant 0.47$ (coded PZT$x \times 100$ for this paper) have previously been determined by x-ray and neutron diffraction [2]. The room-temperature phase $F_{R(LT)}$ is ferroelectric and possesses the space group $R3c$. This phase

‖ Present address: School of Industrial and Manufacturing Science, Cranfield University, Cranfield, Bedfordshire MK43 0AL, UK.

0953-8984/98/081767+20$19.50  

is characterized by cation displacements along $[111]_p$ combined with antiphase octahedral rotations, denoted as $a^-a^-a^-$ (Glazer's notation [3]). This leads to a doubled unit cell in all three directions. This phase transforms on heating (at a temperature depending on composition) into a ferroelectric phase with no octahedral tilts ($a^0a^0a^0$) but with the $[111]_p$ displacements retained and the space group $R3m$, usually denoted as $F_{R(HT)}$. Further heating transforms the structure into the perovskite cubic ($P_C$) phase in which there are neither tilts nor cation displacements.

Electron diffraction studies of these phases have previously revealed the existence of superlattice reflections $\frac{1}{2}\{hkl\}_p$ and $\frac{1}{2}\{hk0\}_p$ (where $h, k, l = 2n + 1$) in the rhombohedral phases of PZT [4–8]. Viehland *et al* [4–7] state that these reflections are the consequence of the condensation of optical phonon modes, either at the R or the M point of the Brillouin zone boundary, which results in different systems of oxygen octahedral tilting. The tilting is ordered either locally or on a 'long-range' scale. The first model, denoted as the R-type tilted system, consists of octahedra alternately rotated clockwise and anticlockwise about $\langle 001\rangle_p$ in successive oxygen layers, characteristic of the $F_{R(LT)}$ phase. This results in a doubling of the unit cell along the $c$ axis and, also, due to successive rotations of the nearest-linked octahedra in the $(001)_p$ plane, doubling of the $a$ and $b$ unit-cell parameters, producing the superlattice reflections $\frac{1}{2}\{hkl\}_p$. The other system, denoted as the M-type tilted system, with rotations about $[001]_p$ for successive oxygen layers in the same sense, is postulated to be responsible for the appearance of $\frac{1}{2}\{hk0\}_p$ reflections. The rotation of the octahedra results again in doubling of the $a$ and $b$ cell parameters, but, as successive octahedra are rotated in the same sense about $[001]_p$, the $c$ parameter is not doubled. This system of octahedral tilting results in tetragonal symmetry. However, with the possibility of microtwins along equivalent $\langle 001\rangle_p$ directions, local tetragonal symmetry could still show 'average' rhombohedral symmetry on a macroscopic scale.

Now, according to Glazer [3] the interpretation of these superlattice reflections in terms of tilted octahedra requires considerable care. For convenience in what follows, we shall group the reflections into four classes: $R_1$, $R_2$, $M_1$ and $M_2$, as shown in table 1. Glazer showed that the antiphase rotations of regular octahedra (e.g. $a^0a^0a^-$ tilts) corresponding to the R-type system give rise to $R_2$ reflections, while in-phase rotations (e.g. $a^0a^0c^+$) of the M-type tilting system give rise to $M_2$. On the other hand, $M_1$ and $R_1$ reflections are not consistent with tilted octahedra, and so, if present, must result from a different structural feature. However, the results reported by Viehland *et al* [4–7] show that the superlattice reflections in the electron diffraction patterns are observed for all values of $h$, $k$ and $l$, and so their interpretation in terms of tilted octahedra alone cannot be correct. It is worth stressing here also that both $M_1$- and $M_2$-type reflections are entirely inconsistent with rhombohedral symmetry.

**Table 1.** Classification of superlattice reflections found in the rhombohedral phase of PZT.

| Type | Reflection | Conditions | Tilt |
|---|---|---|---|
| $R_1$ | $\frac{1}{2}\{hkl\}_p$ | $h = k = l$ | None |
| $R_2$ | $\frac{1}{2}\{hkl\}_p$ | $h \neq k \neq l$ | $a^-$ |
| $M_1$ | $\frac{1}{2}\{0kl\}_p$ | $k = l$ | None |
| $M_2$ | $\frac{1}{2}\{0kl\}_p$ | $k \neq l$ | $a^+$ |

According to Reaney *et al* [9], double-diffraction effects can account for the appearance of the forbidden reflections in most cases. However, in the particular case of the $M_1$

reflections on the $[110]_p$ zone axis diffraction pattern, there is no double-diffraction route to generate them. Therefore, Reaney *et al* [8] suggest, as the most likely explanation for the appearance of the M-type reflections, the presence of anti-parallel cation displacements within the structure. There has never been evidence of $M_1$, $M_2$ or $R_1$ reflections from x-ray or neutron diffraction experiments, only $R_2$ reflections being observed.

In order to clarify the origin and the characteristics of the superlattice reflections in the rhombohedral phase of PZT, electron diffraction combined with TEM dark-field experiments were carried out, and considered along with neutron powder diffraction data and Rietveld powder profile refinement [10]. From the results obtained, we suggest that the most plausible mechanism for the generation of the superlattice reflections is antiparallel displacements of cations in localized regions.

## 2. Experimental procedure

Ceramics of composition $Pb(Zr_{1-x}Ti_x)O_3$, with $x = 0.06$ to 0.45, were sintered from powder prepared by the conventional mixed-oxide method, pressed into pellets and sintered at 1573 K for 5 h. Single crystals of similar compositions were grown from a flux using the system $PbO–B_2O_3$ as a solvent. Previous polycrystalline preparations of $PbZrO_3$ and $PbTiO_3$ were taken in the molar proportions 0.764:0.204:0.024:0.008 ($PbO:B_2O_3:PbZrO_3:PbTiO_3$) and soaked in a platinum crucible at 1313 K for 4 h. During crystal growth, a vertical temperature gradient of 10 K $cm^{-1}$ was maintained. The crucible was then cooled at 8 K $cm^{-1}$ until a temperature of 1173 K was reached, at which point the solvent was poured out. The crystals were then cooled to room temperature and separated from the crucible by soaking in an aqueous solution of acetic acid.

Transmission electron microscopy (TEM) specimens were prepared from 3 mm ceramic discs, which were mechanically polished to 200 $\mu$m thickness and then dimpled in the centre of the disc to 20 $\mu$m. Selected single crystals were gently polished to 10 $\mu$m and mounted onto copper grids. This was followed by further thinning to electron transparency by $Ar^+$ ion milling at 5 kV. Although special care was taken during the preparation of TEM samples, using a low angle (7°) and a cooling stage during the ion milling process, a second polycrystalline phase appeared to develop at the edges of the samples during the final stages of the processing. Traces of the diffraction rings corresponding to this phase can be seen in the electron diffraction patterns. For the TEM studies we used a Philips CM20 microscope working at 200 kV. Heating experiments were carried out at the Manchester Materials Science Centre (UMIST, UK) on an equivalent microscope and using a double-tilt hot-stage holder.

Neutron diffraction data were collected on PZT06 powder using the diffractometer D1A at the Institut Max Von Laue–Paul Langevin (Grenoble, France). The sample was held in a cylindrical vanadium holder (height 6 cm, diameter 1 cm) while data were collected to $\theta_{max} = 79.48°$, with 0.025° steps and $\lambda = 1.907\,88$ Å. The program FULLPROF [11] was used for Rietveld refinement with neutron scattering factors $b_{Pb} = 9.405$ fm, $b_{Zr} = 7.160$ fm, $b_{Ti} = -0.3438$ fm and $b_O = 5.803$ fm. The background was corrected by linear interpolation between 30 given points, while the peak shapes were described by pseudo-Voigt profiles. The initial atomic co-ordinates were taken from the structure determination of rhombohedral PZT by Glazer *et al* [12]. The $R$ factor converged quickly to the values $R_{prof} = 4.65\%$ with $\chi^2 = 2.23\%$. Further experimental details are summarized in table 2. Note the refinement is performed in an associated hexagonal cell, as described by Megaw and Darlington [13].

**Table 2.** Neutron experimental details.

| Experimental data | | | |
|---|---|---|---|
| Chemical formula | $Pb(Zr_{0.94}Ti_{0.06})O_3$ | Space group | $R3c$ |
| $a$ (Å) | 5.8613 (1) | $\alpha$ (°) | 90.00 |
| $b$ (Å) | 5.8613 (1) | $\beta$ (°) | 90.00 |
| $c$ (Å) | 14.4583 (3) | $\gamma$ (°) | 120.00 |
| $Z$ | 8 | $V$ (Å$^3$) | 430.2 |
| Radiation | neutrons | $\theta$ range (°) | 0.0–79.745 |
| Wavelength (Å) | 1.907 88 | Temperature (K) | 293 |

| Data collection | |
|---|---|
| Diffractometer type D1A, ILL | Sample container vanadium holder |
| Monochromator germanium | Instrument geometry 25 $^3$He detectors |
| $2\theta$ step (°) 0.05 | $\theta_{max}$ (°) 79.475 |

| Refinement | | | |
|---|---|---|---|
| Background linear interpolation | | $\chi^2$ 2.23 | |
| $R$ | 4.95 (conventional L.S. refinement) | No of parameters used 24 | |
| | 10.6 (conventional Rietveld $R$ factor) | | |
| $wR$ | 6.93 (L.S. refinement) | Full width at half maximum | |
| | 11.2 (conventional Rietveld $R$ factor) | $u\tan^2\theta + v\tan\theta + w$ | |
| $R_{exp}$ | 4.65 (L.S. refinement) | Weighting scheme $\omega = (\sigma^2)^{-1}$ | |
| | 7.53 (conventional Rietveld $R$ factor) | | |
| $(\Delta/\sigma)_{max}$ | 0.1 | Analytic function for profile pseudo-Voigt | |

## 3. Experimental results

The electron diffraction patterns of PZT06 ceramics, in the low-Ti-level rhombohedral region of the phase diagram, show in most grains the appearance of extra spots of type $R_1$, $R_2$, $M_1$ and $M_2$, as shown in figure 1. The $[0\bar{1}1]_p$ zone axis was chosen because it shows both types of reflection simultaneously. Selecting different areas in the same grain gives rise to changes in the relative intensities of these spots, resulting in patterns with only one type of extra spot for specific regions of the grain, as shown in figures 1(a) and (b). In the latter, only M-type superlattice reflections can be seen, in contrast to the appearance of both R and M types of reflection in the former. In some cases the extra spots completely disappear, as the example of figures 1(c) and (d) shows. In figure 1(c), a region of the grain presents clear reflections at R-type positions only, but when a different area is selected none of these extra reflections are present (figure 1(d)). These results indicate the local character of the structural distortions, typically on a scale of 1–2 $\mu$m, which causes the appearance of these reflections.

Analysis of ceramics with other compositions within the rhombohedral region reveals that the appearance of the superlattice reflections is connected with the Ti content. For PZT12 ceramics, most grains show extra spots only at R-type positions in the $[0\bar{1}1]_p$ zone axis diffraction pattern (figure 2(a)). When the Ti content is close to the morphotropic phase boundary, PZT45, no superlattice reflections are seen (figure 2(b)).

In order to establish whether the appearance of these superlattice reflections is related to some special character of the ceramics, electron diffraction studies were carried out on single crystals in the rhombohedral region. These show the appearance of superlattice reflections at both M- and R-type positions (figure 2(c)), indicating that these superlattice reflections are directly linked to the crystalline structure of the material and do not depend

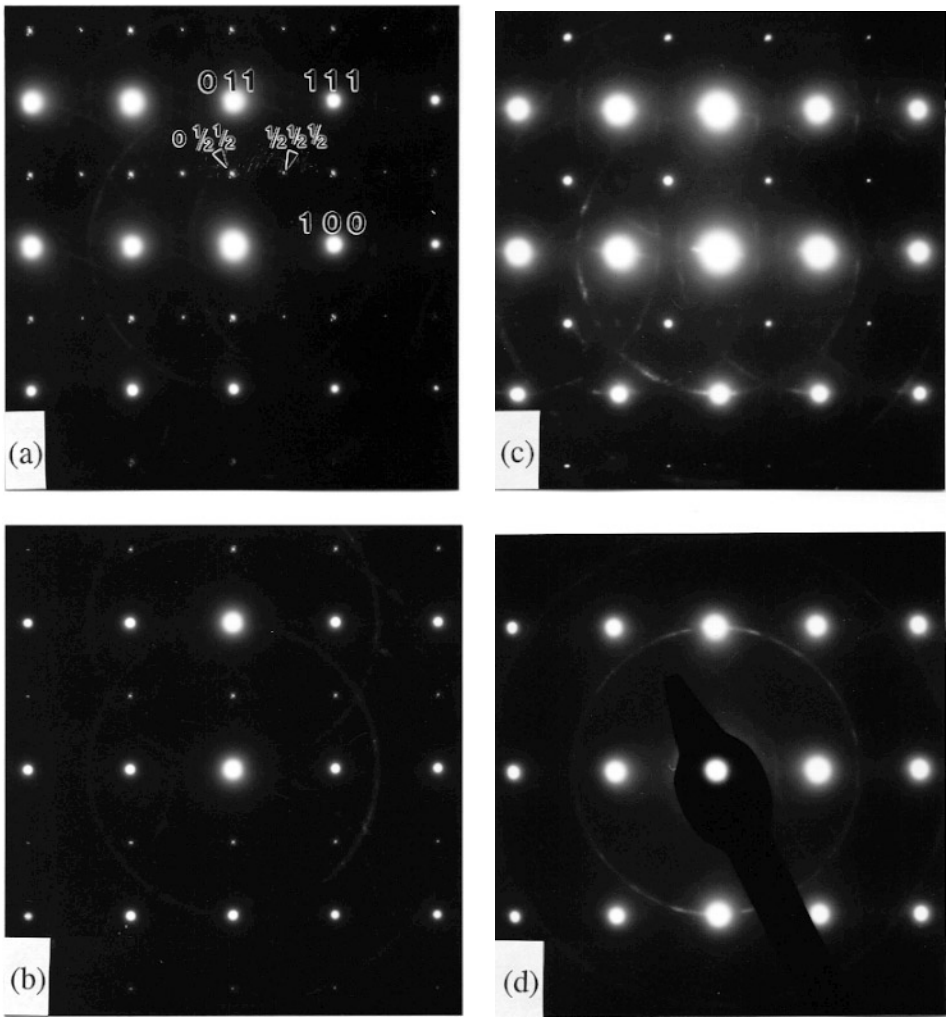


**Figure 1.** $[0\bar{1}1]_p$ zone axis diffraction patterns from PZT06 ceramics. (a) and (b) correspond to different regions of the same grain. Similarly, (c) and (d) show the differences between regions in another grain. In (a), $\frac{1}{2}\{hk0\}_p$ and $\frac{1}{2}\{hkl\}_p$ superlattice reflections are clearly visible. In (b) and (c), only $\frac{1}{2}\{hk0\}_p$ and $\frac{1}{2}\{hkl\}_p$ superlattice reflections are present respectively. In (d) there are no superlattice reflections present.

on the final form of the material, i.e., ceramic or single crystal. It could be contended that the TEM specimen preparation might have introduced the extra reflections. However, specimens were prepared via two different routes: polishing followed by ion thinning and crushing. Superlattice reflections were observed for both cases. It is therefore unlikely that the preparation alone is responsible for them.

The development with temperature of the M-type superlattice reflections for a PZT06 ceramic is shown in figure 3. The extra spots become weaker as the temperature is increased to near the ferroelectric–paraelectric transition (526 K), and they are not visible well above the transition (623 K). On decreasing the temperature, they appear again at 522 K, with highest intensity at room temperature. These observations are in agreement with those

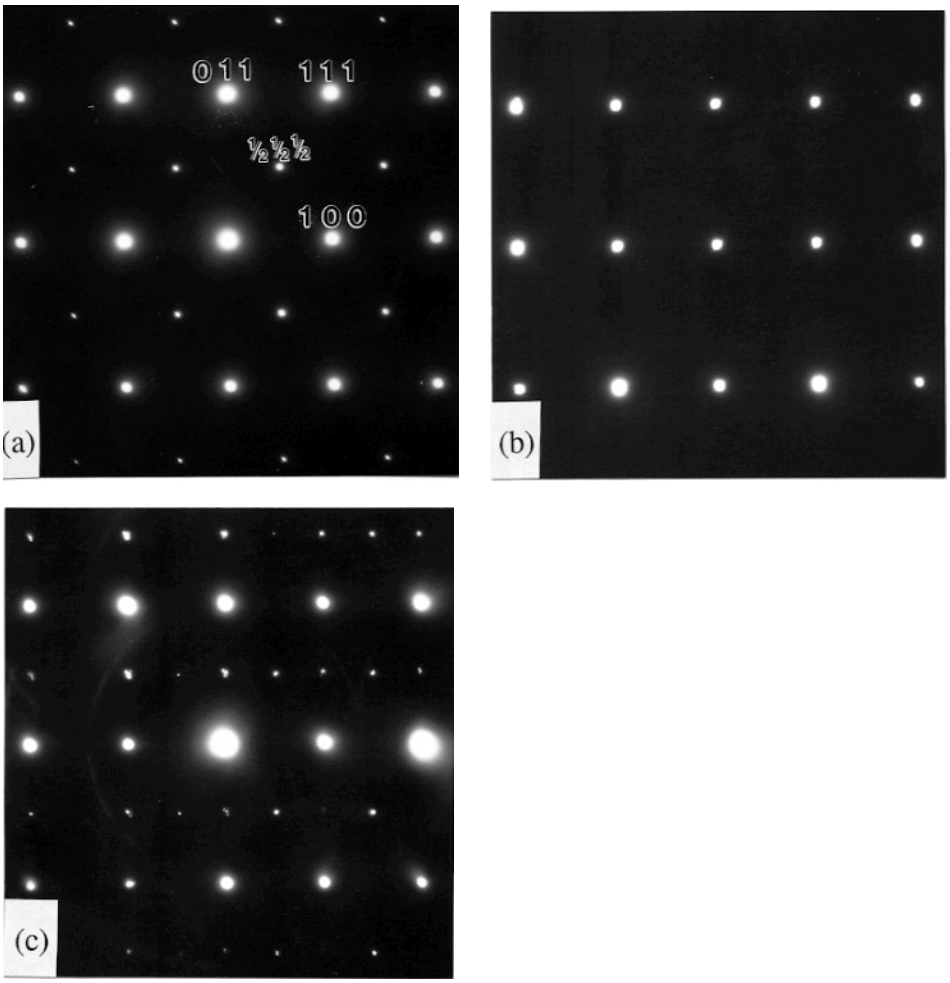


**Figure 2.** $[0\bar{1}1]_p$ zone axis diffraction patterns for different compositions. (a) PZT12 ceramic. (b) PZT45 ceramic. (c) PZT single crystal.

reported in the literature [4–6]. It was observed [6] that for compositions PZT10 and PZT15, only $R_1$- and $R_2$-type reflections appear below the $F_{R(LT)} \rightarrow F_{R(HT)}$ transition temperature, and disappear above it, where only the M-type reflections can be seen.

If we look in detail at these superlattice reflections, we find that those at the M-type positions are accompanied by satellites (figure 4), while the R-type reflections have none. In this particular zone axis, all the satellites are at the same distance from the superlattice spots, following $\langle 110 \rangle_p$ directions. Similar satellites, but following different directions, are observed in other zone axes. They do not show significant changes on going to high-order reflections and are not seen around any of the main reflections. An interesting characteristic of the satellites around the superlattice reflections is the fact that a decrease in the selected area resulted in a decrease of the intensity of one of the pairs of opposite satellites, as shown in figure 4(b). Another important observation is that the superlattice spots observed on the single crystals (figure 2(c)) do not have any satellite reflections. The relevance of these characteristics will be discussed below.

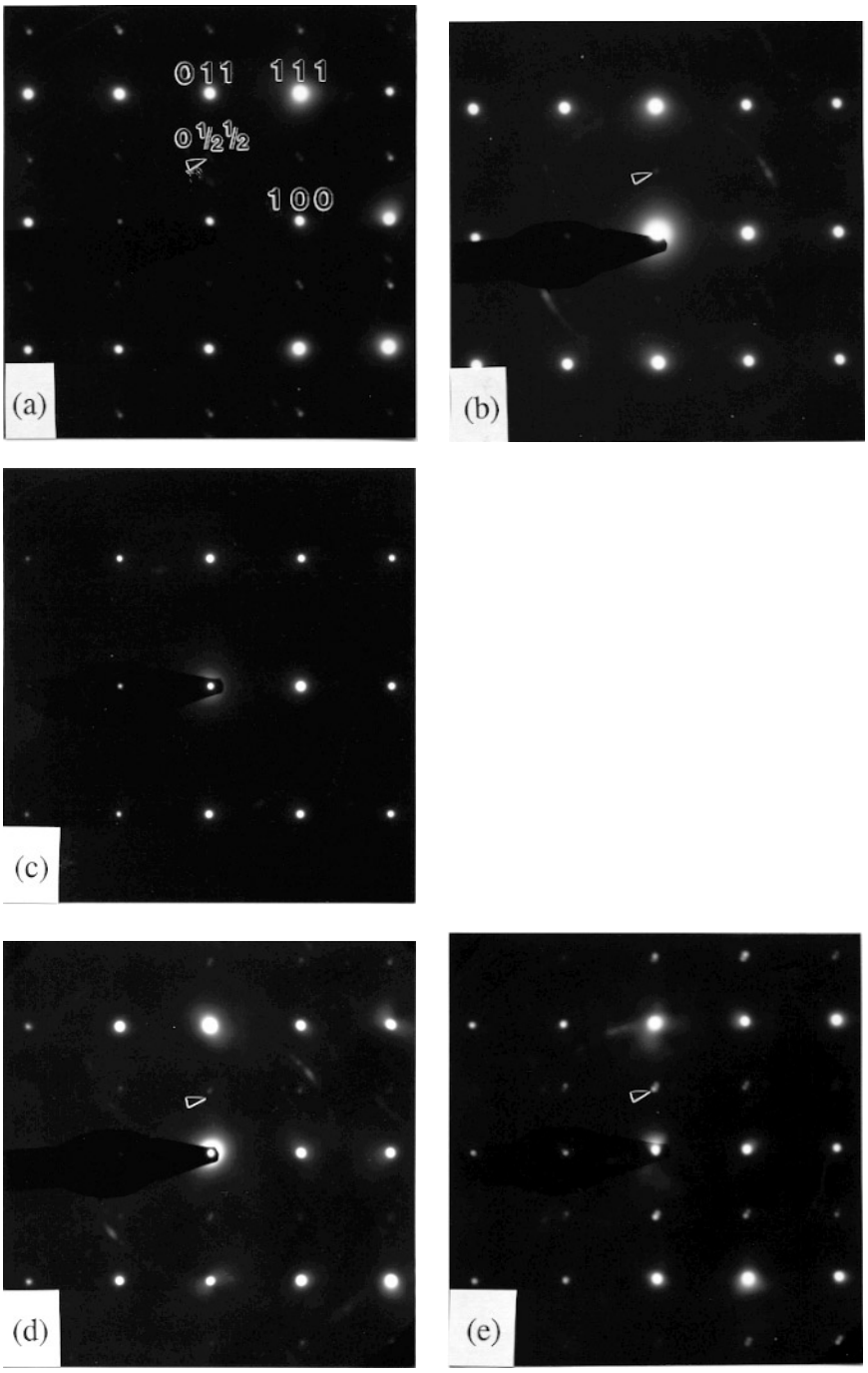


**Figure 3.** Evolution of the $[0\bar{1}1]_p$ zone axis diffraction patterns of a PZT06 ceramic with temperature: (a) 296 K, (b) 526 K (heating), (c) 623 K (heating), (d) 522 K (cooling) and (e) 300 K (cooling).

In order to study the physical features associated with the superlattice reflections, dark-field imaging experiments were carried out. Figure 5 shows a dark-field image from a grain

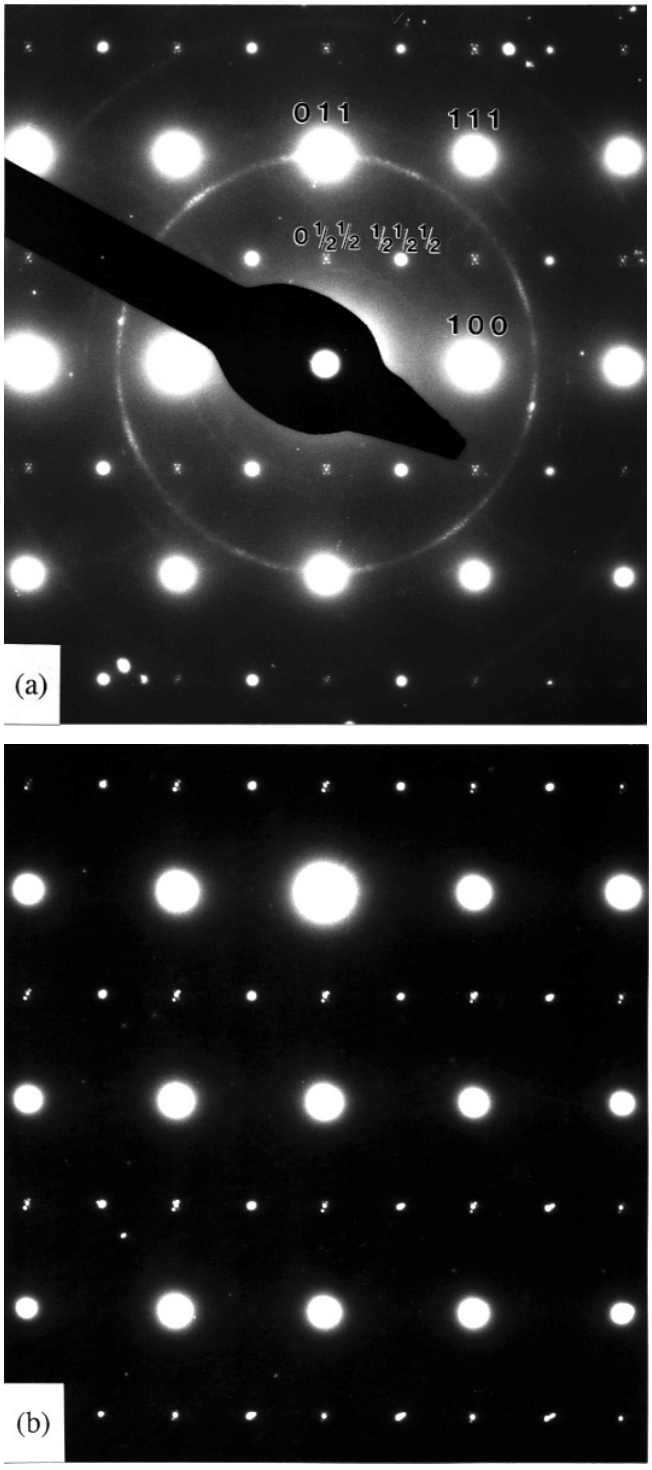


**Figure 4.** Detail of the superlattice spots in a $[0\bar{1}1]_p$ zone axis diffraction pattern showing satellites around the spots at $\frac{1}{2}\{hk0\}_p$, with different apertures of the selected area. (a) Selected area of 6 $\mu$m diameter. (b) Selected area of 1 $\mu$m diameter.

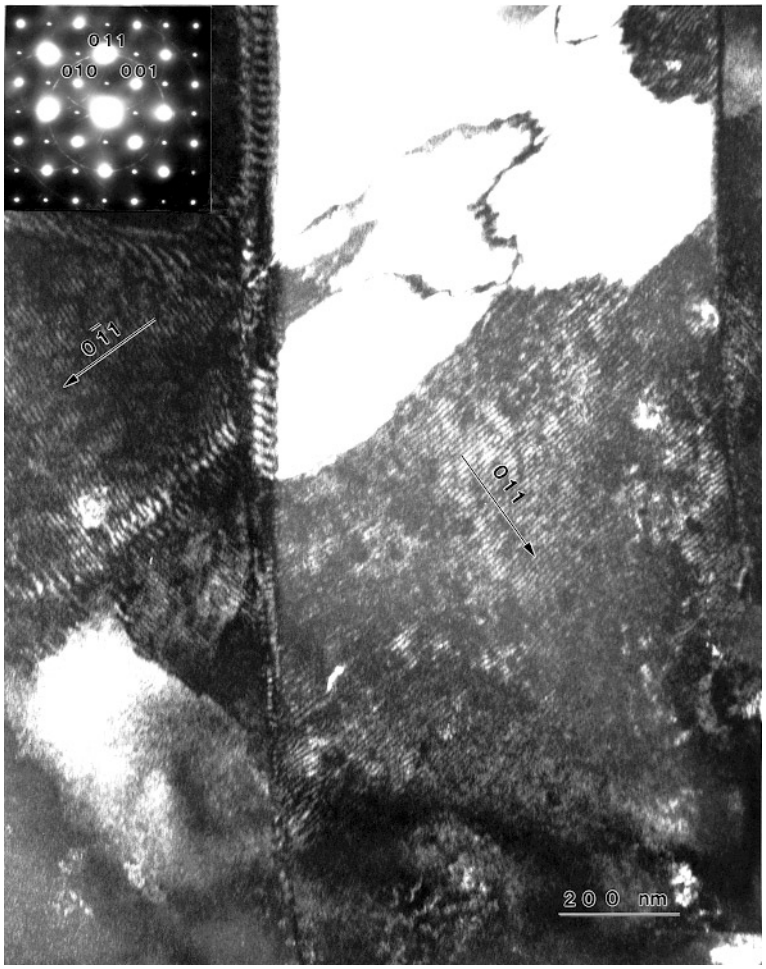


**Figure 5.** Dark-field image of a PZT06 ceramic obtained with the $\frac{1}{2}(110)_p$ superlattice reflection.

in a PZT06 ceramic obtained using an M-type reflection ($\frac{1}{2}(110)_p$). The beam is parallel to $[100]_p$. The picture shows adjacent ferroelectric domains separated by $\{110\}_p$ walls, usually called 109° domains. In these domains, we observe a fine structure of parallel fringes perpendicular to the $\langle 011\rangle_p$ directions and spaced at 10 nm. A change in direction of the fringes from one domain to the other can be seen. In some regions, for example the top right area of the image, typical irregular antiphase boundaries appear. The ferroelectric domain walls exhibit wider fringes, which can be identified as a Moiré effect resulting from the superposition of neighbouring ferroelectric domains. The satellite points around the superlattice reflections in the diffraction pattern follow the same $\langle 011\rangle_p$ directions as the fringes. Furthermore, the spacing of the fringes corresponds to the distance of the satellites to the superlattice reflections in the diffraction pattern. These facts confirm the relationship between the satellite points observed in the diffraction pattern and the parallel fringes shown in the bright-field image. Fringes showing similar characteristics are found on looking along other zone axes.

In contrast to the above, dark-field experiments carried out with an R-type superlattice reflection ($\frac{1}{2}(111)_p$) do not show any fringes (figure 6). The lack of satellites around these


**Figure 6.** Dark-field image of a PZT12 ceramic obtained with the $\frac{1}{2}(111)_p$ superlattice reflection.

reflections explains the absence of fringes. Some irregular antiphase boundaries can be seen inside the region from which the R-type superlattice reflection comes. In this example, the large region of the grain contributing to these reflections has produced a reliable dark-field image. Usually, this is not the case, and it is difficult to obtain an image of these regions.

The superlattice reflections are also observed in electron diffraction patterns in other zone axis with higher indices, like $[3\bar{1}\bar{1}]_p$ in figure 7(a). This shows that they are not dependent on the direction of observation. The study of some of these patterns also revealed differences in the intensities between $(001)_p$ and $(002)_p$ reflections, as shown in the $[0\bar{2}1]_p$ pattern of figure 7(b). Such differences are not observed in the $[0\bar{1}\bar{1}]_p$ patterns. This can be attributed to a channelling effect enhancing the intensity of $(001)_p$ reflections in low-index zone axes, where these effects are known to be more important.

As a further investigation into the structure of this phase, figure 8 shows the observed, calculated and difference neutron diffraction profiles for PZT06 powder, simulated using the program Crystallographica [14]. Final positional parameters are given in table 3. Neither these profiles nor previous x-ray studies show any evidence of the existence of M-type reflections (not allowed according to rhombohedral symmetry) or $R_1$ reflections. For instance, we have marked in figure 8 the positions expected for $\frac{1}{2}(110)_p$ ($M_1$-type) and $\frac{1}{2}(111)_p$ ($R_1$-type) reflections. The observed superlattice reflection at $2\theta = 45.2^\circ$ is $\frac{1}{2}(311)_p$ (an $R_2$ reflection) which *is* allowed for the $a^-a^-a^-$ tilted structure. The fact that the superlattice reflections of type $R_1$, $M_1$ and $M_2$ can only be seen using electron diffraction, and not by neutron or x-ray diffraction, is clearly an important point and is discussed further below.

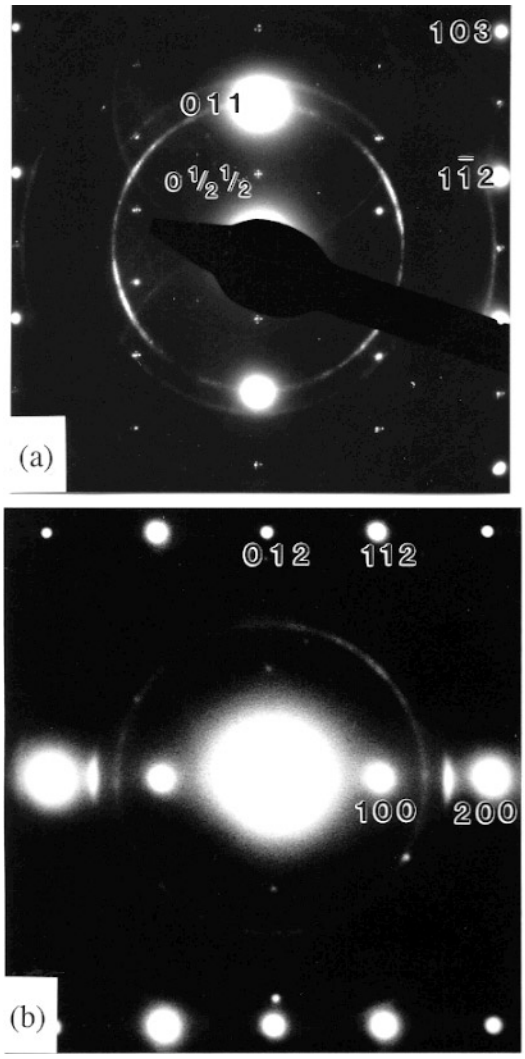


**Figure 7.** Electron diffraction patterns in two zone axes: (a) $[31\bar{1}]_p$ (from a PZT06 ceramic) and (b) $[0\bar{2}1]_p$ (from a PZT12 ceramic).

**Table 3.** Final positional parameters obtained from the neutron diffraction studies on PZT06 powder.

| Atom type | $X/a$ | $Y/b$ | $Z/c$ | Occ. |
|---|---|---|---|---|
| Pb(1) | 0.0000 | 0.0000 | 0.2831(2) | 0.333 |
| Zr(1) | 0.0000 | 0.0000 | 0.0131(3) | 0.299(1) |
| Ti(1) | 0.0000 | 0.0000 | 0.0131(3) | 0.034(1) |
| O(1) | 0.1436(3) | 0.3469(3) | 0.0833 | 1.0 |

## 4. Discussion

The electron diffraction studies carried out in this work reveal many of the characteristics of the superlattice reflections usually observed in the rhombohedral phase of PZT. The fact

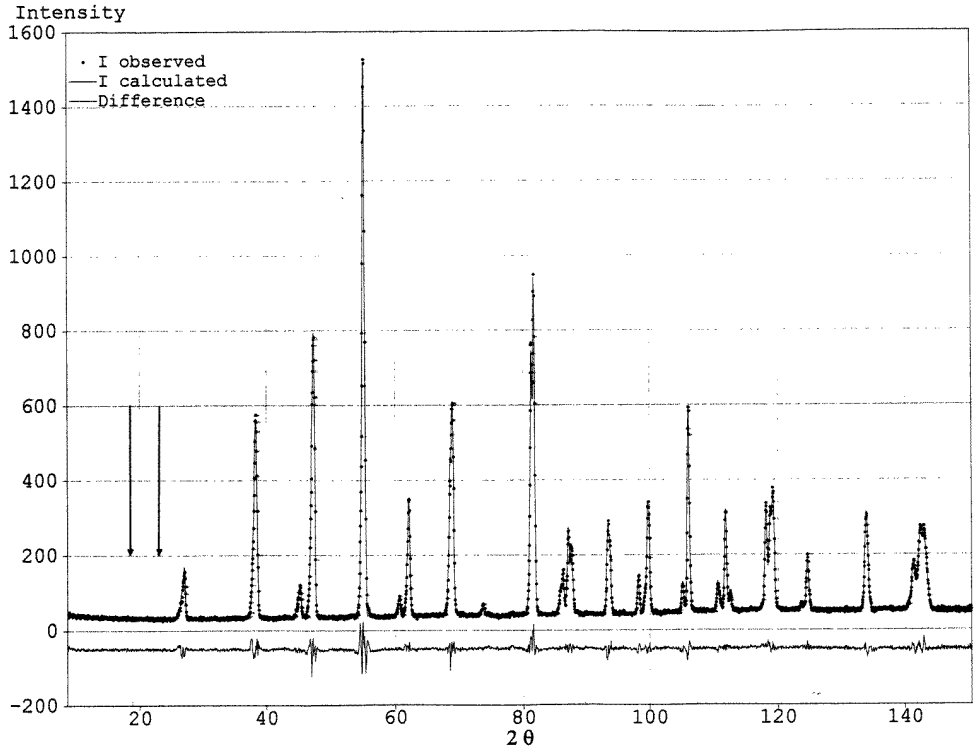


**Figure 8.** Observed, calculated and difference neutron diffraction profiles of PZT06. The arrows indicate the position where the superlattice reflections $M_1$ and $R_1$ should appear.

that the intensity of the extra spots at $M_1$, $M_2$ and $R_1$ positions is dependent on the region of the crystal from which the pattern is taken indicates that the origin of the superlattice is a spatially localized phenomenon in the crystal. It has also been shown that these localized structures appear in single crystals, suggesting that the origin is not related to a particular characteristic of the polycrystalline ceramics, but to a fundamental aspect of the crystal structure in the material. In contrast, however, the satellites around M points do appear to be a characteristic feature of the ceramics and not of the single crystals.

In order to suggest the origin of the extra reflections, electron diffraction simulations of various structural models were made as shown in figure 9. A comparison between the experimental results, i.e. relative intensities and types of extra reflection, and the simulations has allowed us to draw some qualitative conclusions about the local deviations from the 'average structure' of the rhombohedral phase. For different electron diffraction patterns different regions contribute to the intensity of the extra reflections and, hence, it is extremely difficult to quantify the results. For instance, the intensity of the $\frac{1}{2}(111)_p$ ($R_1$) reflection varies from zero intensity to 65% of that of the $(200)_p$ reflection ($I_{200}$). However, although it is therefore not possible to predict the 'local structure' quantitatively, the basic attributes of the possible models can be determined and are discussed below.

The temperature dependence of the extra reflections, especially the fact that they disappear in the cubic paraelectric structure, strongly suggests that they originate from structural features related to the ferroelectric state, i.e. to cation displacements or octahedral tilts, rather than from static contributions such as Zr/Ti ordering.

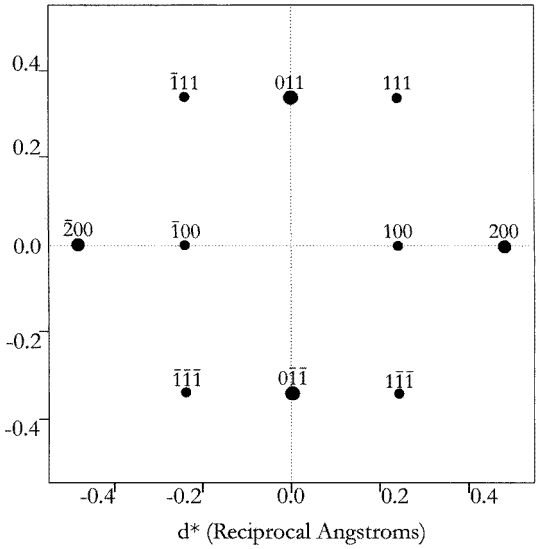


(a)

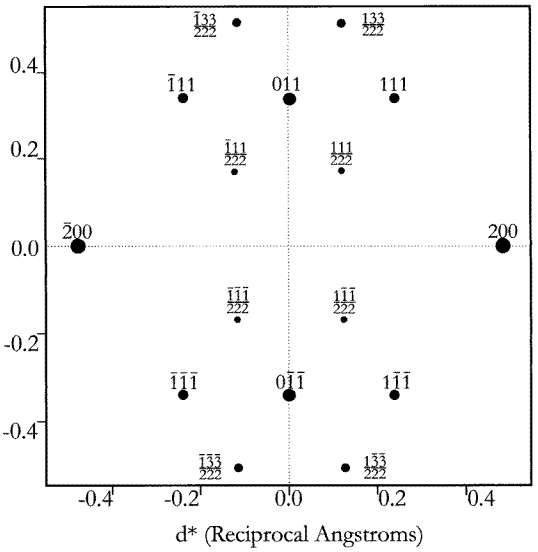


(b)

**Figure 9.** Simulations of $[0\bar{1}1]_p$ zone axis electron diffraction patterns. (a) Average rhombohedral structure. (b) Structure composed of two layers, with antiparallel displacement of cations. (c) Structure composed of one layer, with antiparallel displacement of cations.

Although many possible structural candidates were investigated, the models presented below summarize the most important conclusions. In each case the electron diffraction simulations were generated using the diffraction and microscopy tools of the program Cerius[2] [15]. Initial input models of tilting octahedra systems were formed using the program POTATO (program originated to analyse tilted octahedra) [16].

The first model is based on the average $F_{R(LT)}$ structure observed in the ferroelectric low-temperature rhombohedral region of the PZT phase diagram. As noted in the introduction,

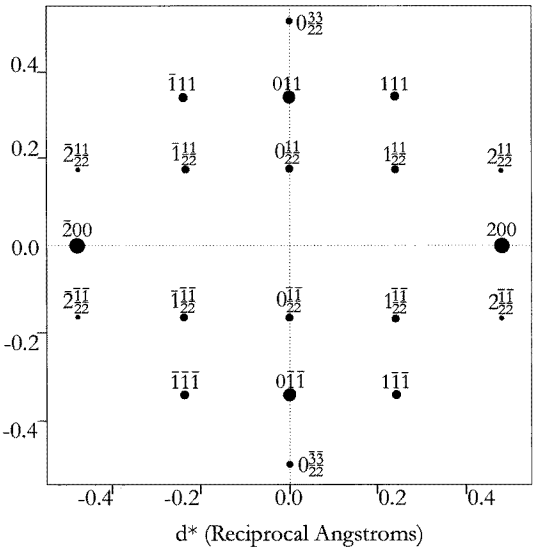


(c)

**Figure 9.** (Continued)

at room temperature the 'average' $F_{R(LT)}$ structure has oxygen octahedra tilted about $[111]_p$, in the $a^-a^-a^-$ tilt system, which results in the cell doubling of all three pseudocubic axes, hence forming a unit cell containing eight formula units. Parallel displacements of the cations occur at the same time along $[111]_p$. Typical values for the angles of tilt of the oxygen octahedra and the displacements of lead atoms from their ideal cubic, high-symmetry positions were initially taken from the determination of the PZT10 structure by Glazer *et al* [12]. However, in some models slightly larger displacements and tilts were used in the hope of exaggerating the superlattice reflections. In the first model a regular $a^-a^-a^-$ octahedron tilt system with 4° tilts around each axis was combined with Pb atoms displaced approximately 0.7 Å along $[111]_p$. The rhombohedral unit cell, defined by the degree of octahedral tilting and Zr–O distance, was formed with $a = 8.3195$ Å, $\alpha = 89.719°$. The associated single-crystal electron diffraction pattern ($\lambda = 0.0251$ Å, 200 kV) zone axis $[0\bar{1}1]_p$ is shown in figure 9(a). The simulation does not show any superlattice reflections at $R_1$ points, the ones at $R_2$ being too weak to be shown, contrary to the predictions of other authors [4–7]. If in the model we use the $a^0a^0c^+$ tilting system instead, which is postulated as the origin of the M-type superlattice reflections, the simulated electron diffraction pattern is equivalent to the previous one, without any extra spots. This confirms that the types of extra reflection observed in the experimental studies are indeed systematically absent for the models based on the rotation of regular octahedra, as predicted by Glazer [3].

One common feature observed in complex perovskites is the distortion of oxygen octahedra. Indeed it could be argued that earlier models [4–7] may still be correct if the octahedra were deformed, rather than regular, as such a break in symmetry would allow more superlattice reflections. Without any criteria for speculating on the possible type of distortion which may be present, a model was formed by generating unequal tilts around the *a*, *b* and *c* axes (2, 7 and 12° respectively) followed by small random translations of the oxygen atoms. $[111]_p$ Pb displacements were kept in the model. These generated highly distorted octahedra of microscopic space group symmetry $P1$ with Zr–O bond distances varying from 1.5 to 2.5 Å. Although physically unrealistic, the extreme octahedra formed were used, as

they represented every possible deviation from regularity. In this case, simulated electron diffraction patterns exhibited R- and M-type reflections, but with negligible intensity (less than 0.05% of $I_{011}$). This is the most important conclusion of the simulations. In brief, by including different types of octahedral distortion in the PZT model it is possible to generate either or both of the $R_1$- and M-type reflections. However, the relative intensities of these reflections are only caused by the oxygen shifts from their high-symmetry, cubic sites and are too weak to be shown on a simulated pattern or to be experimentally observed.

These conclusions are in complete contrast with the conclusions of other authors [4–7], who stated that the $\frac{1}{2}\{hk0\}_p$ and $\frac{1}{2}\{hkl\}_p$ (differentiation between $R_1$, $R_2$, $M_1$ and $M_2$ reflections was not made by these authors) superlattice reflections arise from octahedral tilts of the type $a^0a^0c^+$ and $a^-a^-a^-$, respectively. These simulations show conclusively that octahedral tilts and distortions alone are insufficient to give rise to $R_1$ and M superlattice reflections with the intensities observed.

We are therefore compelled to assume that cation shifts, different from the $[111]_p$ shifts seen in the 'average' structure, are responsible for the generation of the extra reflections. As both the M and $R_1$ sets of reflections are observed independently, they must originate from different types of shift. However, it seems logical to us that, whatever type of shift is responsible for one set of reflections, it is also related in some way to the shift generating the others. This leads us to the final two models presented.

One of the simplest variations on the cation displacements which can cause $R_1$-type reflections is that formed by introducing antiparallel components. Keeping the doubled unit cell ($2a_p \times 2b_p \times 2c_p$) and associated $a^-a^-a^-$ tilt system, this model may be most easily visualized by separating the unit cell into two layers, each of ($a_p \times 2b_p \times 2c_p$) and introducing antiparallel $[011]_p$ displacements of the Pb atoms. The layers and the resulting structure are shown in figure 10. Keeping the rhombohedral unit-cell dimensions unchanged, this simple arrangement of Pb displacements leads to strong $R_1$-type (as well as $R_2$) reflections, as shown in figure 9(b). The exact intensity of the extra superlattice reflections varies with the degree of Pb displacement from its high-symmetry cubic site. For instance, for a displacement of around 0.25 Å the intensity of $\frac{1}{2}(111)_p$ ($R_1$ reflection) is 10% of $I_{200}$, while an increase of displacement to around 0.5 Å (a typical value in this region) leads to an intensity of 37% of $I_{200}$, a value consistent in magnitude with the ranges observed in practice. We call this structure $A_I$. Although there is no further experimental proof that this modification is correct, the model is both physically realistic and also leads to a similar model which could be responsible for the M-type reflections.

On initial examination of this simulation we find that $(100)_p$ reflections disappear for this model, as a result of cancellation between the scattering factors of Pb and Zr. The appearance of these reflections in the experimental diffraction patterns can be explained by the superposition of diffraction from the 'average' rhombohedral and local $A_I$ structure. However, a lower intensity for $(100)_p$ reflections, coming from only one of the phases present, than for $(200)_p$ reflections is expected. This is observed in the diffraction pattern shown in figure 7(b), but not in the $[0\bar{1}1]_p$ zone axis patterns. The intensities of the $(100)_p$ reflections in these patterns can be enhanced by a channelling effect, more important in low-index diffraction patterns like this, producing as a result similar intensities for both reflections. The presence of channelling effects in this particular zone axis should not be related in any case to the appearance of the superlattice reflections, as they are observed in diffraction patterns with a high-order zone axis (figure 7(a)).

In order to generate M-type reflections it is unnecessary to have a full doubled unit cell ($2a_p \times 2b_p \times 2c_p$). Hence, whereas the unit-cell model for $R_1$ reflections is achieved by stacking the depicted layer 1 on top of layer 2 (figure 10), in the case of M reflections only

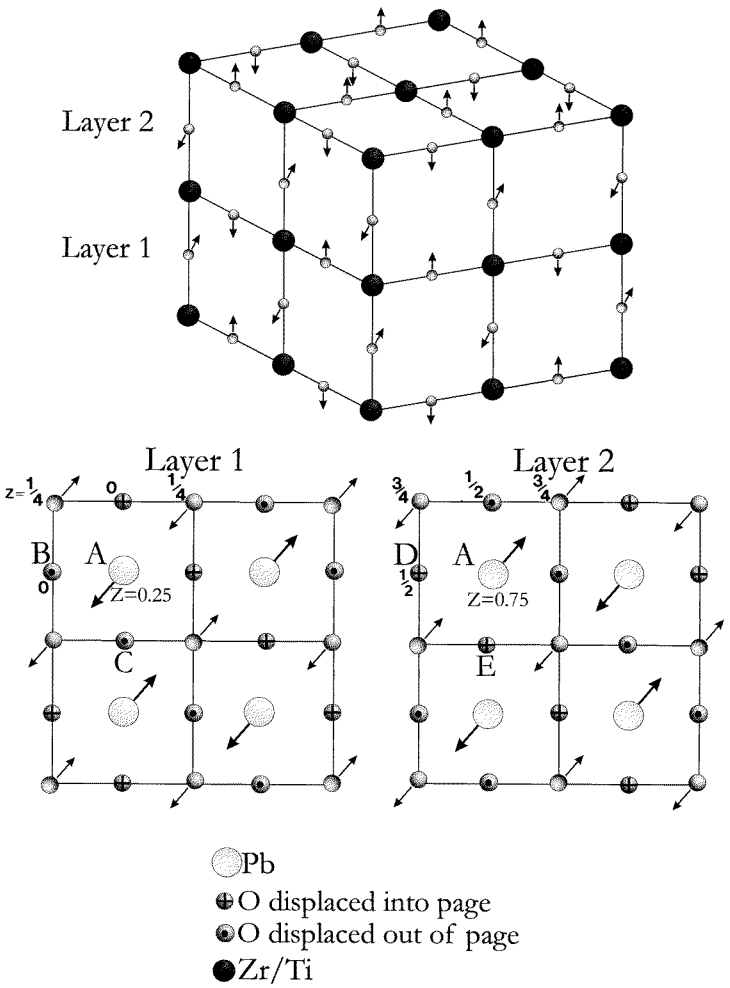


**Figure 10.** Proposed model of the local structures responsible for the appearance of superlattice reflections, introducing antiparallel $[011]_p$ displacements of the Pb atoms. At the top we show a three-dimensional picture of the $A_I$ structure, composed of the two layers shown below, viewed down $[100]_p$.

one of the layers is necessary, i.e., the unit cell has half the volume. An electron diffraction simulation using layer 2 only is shown in figure 9(c). Again the intensity of the simulated $\frac{1}{2}\{011\}_p$ ($M_1$ type) reflections is around 30% of $I_{200}$, for a 0.5 Å cation shift. We refer to this structure as $A_{II}$.

The electron diffraction experiments carried out with samples of different compositions suggest that the appearance of these extra spots is limited to the lower-Ti-level rhombohedral regions. Compositions near the morphotropic phase boundary do not present any of the superlattice reflections (figure 2(b)). Furthermore, an evolution is observed, with the progressive disappearance of the M reflections on going from PZT06 to PZT12, as can be seen by comparing figures 1 and 2(a). This observation is also confirmed in previous works [4–6]. Moving to still higher levels of Ti we also observe the disappearance of the $R_1$ and $R_2$ reflections. For compositions PZT10 and PZT15, these reflections disappear as the temperature is increased and are replaced by the M reflections [4–6].

It has been observed by Corker *et al* [17] that in the antiferroelectric orthorhombic ($A_O$) structure of PZT for $x < 0.05$, the octahedral tilting system is basically a form of $a^-a^-c^0$ with highly distorted octahedra, so that the $Pb^{2+}$ ions can achieve fourfold co-ordination by oxygens. The distortions in the octahedra are quite large with O–O distances varying between 2.81 and 3.12 Å. This is possible because the $Zr^{4+}$ ions are relatively large at 0.72 Å (0.60 Å for $Ti^{4+}$) and tend to push the oxygen ions apart. Analysis of the orthorhombic structure suggests that $Pb^{2+}$ ions prefer to maintain a fourfold co-ordination with oxygens and this may provide an explanation for the antiparallel cation displacements postulated in this paper. Consider first the arrangement of displacements proposed for the structure, $A_I$, which gives rise to the R reflections. It is postulated that if one of the rhombohedral tilts disappears, giving $a^-a^-c^0$, then the arrangement of ionic displacements shown in figure 10 may be produced (heights in the doubled unit cell are given). The $Pb^{2+}$ ion at A in this figure would be brought closer to the oxygens at B, C, D and E, giving the fourfold co-ordination favoured by $Pb^{2+}$. This is true for all the Pb ions in the structure. While there is no direct evidence to support this postulate, such an arrangement of oxygen octahedra, with the loss of one tilt alone, would be relatively easy to accommodate within the existing $a^-a^-a^-$ system. This would accommodate relatively small octahedral distortions and stresses at the interfaces between regions of the crystal with the $F_{R(LT)}$ structure and regions with structure $A_I$. One would therefore think that it would be possible for this structure to persist uniformly within the rhombohedral grains, as is observed, and to be relatively stable when the octahedra become progressively more rigid as the $Zr^{4+}$ ions are replaced by $Ti^{4+}$ ions. Indeed, it is possible to envisage structure $A_I$ as a persistence of the main features of the orthorhombic $A_O$ structure well into the $F_R$ structural region, these features being antiparallel cation displacements along $\langle 110 \rangle_p$ and $a^-a^-c^0$ tilting.

If we now consider the $A_{II}$ structure, considerations of the cation and oxygen displacements in both layers show that it is not possible to accommodate an octahedral tilting system which gives fourfold co-ordination of all the $Pb^{2+}$ by oxygen without large octahedral distortions. This would provide an explanation as to why structure $A_{II}$ is less stable than structure $A_I$ as the Zr is progressively replaced by Ti, i.e. the more rigid the octahedra become, the harder it is for them to accommodate this structure. The two structures proposed also provide an explanation as to why structure $A_I$ becomes less stable than $A_{II}$ as the temperature is raised. At the $F_{R(LT)} \rightarrow F_{R(HT)}$ transition, the $a^-a^-a^-$ tilt system disappears. This may make the $a^-a^-c^0$ tilts postulated for the structure $A_I$ less stable. The lattice also expands with increasing temperature, making the octahedra more tolerant to the $A_{II}$ structure.

This explanation of the origins of the M and $R_1$ reflections in terms of distinct structures with different antiparallel cation displacements along $\langle 110 \rangle_p$ could also provide an explanation for the origins of the satellite reflections around the M reflections, but not around R. These satellites appear in pairs along $\langle 110 \rangle_p$ and have their origin in periodic antiphase boundaries running along $\langle 110 \rangle_p$ and possessing a periodicity of 10 nm. These can only occur for the $A_{II}$ structure, since this gives rise to the M-type reflections. It is interesting to consider the structure around one of these boundaries. Figure 11 shows Pb ion displacements in one layer of the $A_{II}$ structure (the next layer up being the same). Here, we have introduced an antiphase boundary along AB, in this case forming a $\{110\}_p$ mirror/glide plane in the structure. Consider, now, the Pb ion displacements in the $A_O$ structure of $PbZrO_3$ [17] which are shown diagrammatically in figure 12. Here, again, we have shown only one layer of the structure (the next layer of cations along $z$ possesses similar displacements). The projection of the orthorhombic unit cell on $(001)_p$ is marked. It is easy to see that the structure between the $\{110\}_p$ planes CD and EF straddling the

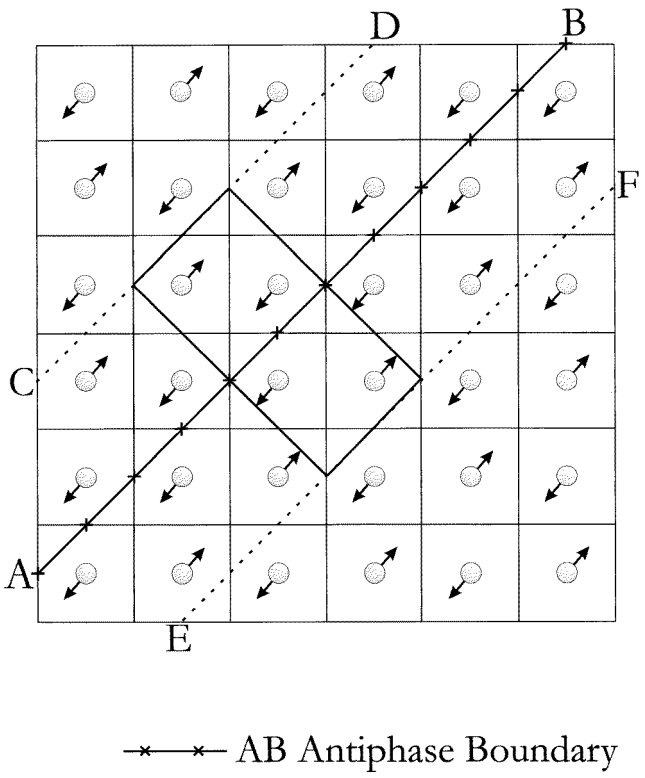


**Figure 11.** An antiphase boundary in a structure of the type postulated for $A_{II}$, showing the appearance of a structure similar to the $PbZrO_3$ $A_O$ phase around the antiphase boundary in the region between the lines CD and EF.

antiphase boundary in figure 11 is identical to the orthorhombic $PbZrO_3$ structure shown in figure 12 (the corresponding orthorhombic $PbZrO_3$ unit-cell projection is marked). It seems likely that the oxygen octahedron tilts in this region could be a distorted form of $a^-a^-c^0$, as in $A_O$ $PbZrO_3$. This also tends to support the postulate that these regions of structure possessing antiparallel cation displacements occur because the structure is trying to preserve the features of the $PbZrO_3$ $A_O$ phase. We therefore envisage that the areas of the sample, which produce the {110} satellite reflections, consist of periodic antiphase boundaries, which are regions possessing the $PbZrO_3$ $A_O$ structure, running parallel to $\langle 110 \rangle_p$ and separated by about 10 nm of $A_{II}$ structural material. Such an ordered state is not always found, as the irregular antiphase boundary at the top of figure 5 and the absence of satellites around the superlattice reflections in the single crystal show.

An important issue raised by the observations reported here is that the superlattice reflections of type M and $R_1$ are not seen by either neutron or x-ray diffraction, but only by electron diffraction. We can consider several reasons for this. First of all, the superlattice reflections may be too weak in either neutron or x-ray diffraction to be seen because of the difference in scattering factors for the different radiations. This has been shown by simple simulations to be incorrect for the structural models of the type $A_I$ or $A_{II}$. Further initial consideration is that the volumes of structures giving rise to the superlattice reflections are much smaller than the $F_R$ phase so that the reflection intensities are again too weak to be seen by neutron or x-ray diffraction. They are observed by electron diffraction because the

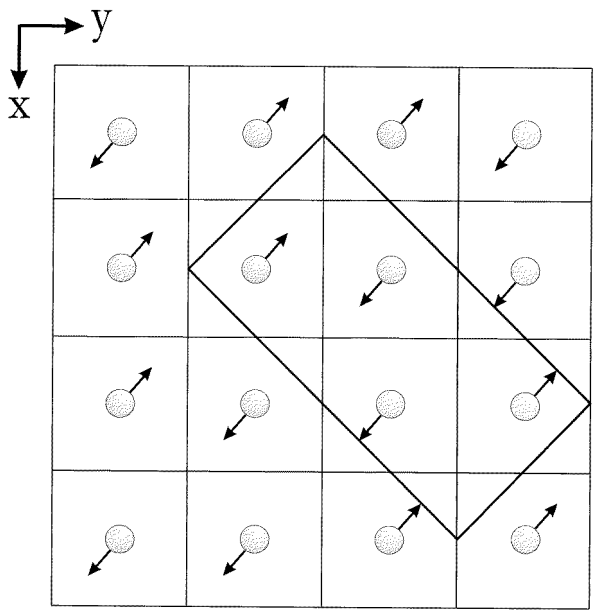


**Figure 12.** One layer of the $PbZrO_3$ $A_O$ structure showing the Pb displacements and the projection of the orthorhombic unit cell on $[001]_p$.

technique examines very small areas. This is possible, but unlikely, because observations on all the samples show that regions showing either or both types of superlattice reflection are easy to find. It is estimated that these regions must amount to about 70% of the sample for PZT06, and hence should be seen in both the x-ray or neutron methods. It must also be considered whether the crystallite regions giving rise to the superlattice reflections may be so small that particle size broadening effects for the longer-wavelength x-rays and neutrons make the reflections unobservable against the background. This would imply a particle size of approximately 1 nm. The dark-field images presented in figures 5 and 6 suggest that this is not the case.

What also must be taken into account is the fact that the TEM specimens are different from the x-ray and neutron specimens, which may be the reason for the appearance of the superlattice reflections in the former and not in the latter. The most plausible reason for this is that the TEM specimens are very thin (typically between 50 and 500 nm). It is possible that the structures we observe in the TEM specimens are dominated by their surfaces [18], depressing the stability of the ferroelectric phase. It may well be that this effect allows the antiparallel cation displacements that we have postulated for structures $A_I$ and $A_{II}$ to become stable in the regions of the phase diagram, where the Ti ion substitutions for Zr have not made the octahedra too rigid†.

## 5. Conclusions

The evidence for the appearance of the superlattice reflections of the type M and $R_1$ in electron diffraction patterns of rhombohedral $Pb(Zr_{1-x}Ti_x)O_3$ for $0.06 \leqslant x \leqslant 0.42$ has been

† New data from neutron diffraction studies have produced more accurate information about the displacements of the cations, which is unobtainable from electron diffraction studies. Based on this new evidence, Corker *et al* propose some modifications to the present models, which will be submitted shortly to this journal.

presented. It has been shown that these reflections come from localized regions either in a single crystal or a ceramic. An increase in the Ti content results in the disappearance of these extra reflections, firstly the M reflections, and then the $R_1$ reflections. Regarding the temperature dependence, these reflections disappear when the paraelectric phase is reached. Satellites are found only around the M reflections and are related to $\langle 110 \rangle_p$ antiphase boundaries. None of these superlattice reflections are observed by neutron diffraction.

The observation of extra reflections agrees with that presented by other authors [4–8]. However, it has been demonstrated that rigid octahedral tilts alone are insufficient to give rise to the observed intensities and two models involving antiparallel displacements of the Pb ions have been postulated which are fully consistent with the observations. Satellite spots around the M-type superlattice reflections are most likely to be caused by periodic antiphase boundaries occurring in one of these phases, which are probably stabilized by the similarity of the structure in the region of the antiphase boundary to the $A_O$ phase of $PbZrO_3$. Reasons for the superlattice reflections to occur uniquely in electron (and not neutron or x-ray) diffraction have been considered and it is postulated that the structures causing them are caused by surface effects in the TEM specimens.

## Acknowledgments

The authors wish to acknowledge Mr A M Stallard (Cranfield University) for ceramic preparation and the assistance of Mr P Kenway (UMIST, Manchester, UK). We would also like to thank the Institut Max Von Laue–Paul Langevin (ILL) (Grenoble, France) for the use of facilities for the neutron diffraction studies. We also like to thank Professor D Barber for useful discussions. One of the authors, Dr D L Corker, also expresses gratitude to Dr F Fauth for his assistance during her time at the ILL and for his continuing help. Professor R W Whatmore gratefully acknowledges the financial support of the Royal Academy of Engineering. This work was funded by the Engineering and Physical Sciences Research Council (EPSRC).

## References

[1] Reaney I M 1996 *Proc. Electroceram.* **1** 441–6
[2] Michel C, Moreau J M, Achenbach G D, Gerson R and James W J 1969 *Solid State Commun.* **7** 865–8
[3] Glazer A M 1975 *Acta Crystallogr.* A **31** 756–62
[4] Viehland D, Li J-F, Dai X and Xu Z 1996 *J. Phys. Chem. Solids* **57** 1545–54
[5] Viehland D 1995 *Phys. Rev.* B **52** 778–91
[6] Dai X, Xu Z and Viehland D 1995 *J. Am. Ceram. Soc.* **78** 2815–27
[7] Xu Z, Dai X, Li J-F and Viehland D 1995 *Appl. Phys. Lett.* **66** 2963–5
[8] Reaney I M, Glazounov A, Chu F, Bell A and Setter N 1997 *Br. Ceram. Proc.* **57** 17–33
[9] Reaney I M, Colla E L and Setter N 1994 *Japan. J. Appl. Phys.* **33** 3984–90
[10] Rietveld H M 1969 *J. Appl. Crystallogr.* **2** 65
[11] Rodriguez-Carvajal J 1995 *FULLPROF. A Rietveld Refinement and Pattern Matching Analysis Program* (Laboratoire Leon Brillouin, Lyon, CEA–CNRS)
[12] Glazer A M, Mabud S A and Clarke R 1978 *Acta Crystallogr.* B **34** 1060–70
[13] Megaw H D and Darlington C N W 1975 *Acta Crystallogr.* A **31** 161–7
[14] Oxford Cryosystems 1996 *Crystallographica. A Crystallographic Data Software Tool*
[15] Molecular Simulations 1995 *Cerius*$^2$*. Graphics and Diffraction Simulation Tool*
[16] Woodward P M 1997 *J. Appl. Crystallogr.* **30** 206–7
[17] Corker D L, Glazer A M, Dec J, Roleder K and Whatmore R W 1997 *Acta Crystallogr.* B **53** 135–42
[18] Känzig W 1955 *Phys. Rev.* **98** 549–50